Radiogenic helium isotope fractionation: The role of tritium as He-3 precursor in geochemical applications

Article *in* Geochimica et Cosmochimica Acta · May 1999

DOI: 10.1016/S0016-7037(99)00105-2

CITATIONS
19

READS
37

9 authors, including:

Igor Tolstikhin
Kola Scientific center RAS, Apatity
145 PUBLICATIONS **3,559** CITATIONS
SEE PROFILE

Valentin Nivin
Kola Science Centre
37 PUBLICATIONS **457** CITATIONS
SEE PROFILE

Igor Tokarev
Saint Petersburg State University
62 PUBLICATIONS **207** CITATIONS
SEE PROFILE

Maria Gannibal
Kola Science Centre
24 PUBLICATIONS **231** CITATIONS
SEE PROFILE

Pergamon

Geochimica et Cosmochimica Acta, Vol. 63, No. 10, pp. 1605–1611, 1999

0016-7037/99 $20.00 + .00

PII S0016-7037(99)00105-2

Radiogenic helium isotope fractionation: The role of tritium as ^{3}He precursor in geochemical applications

I. N. Tolstikhin,[1] B. E. Lehmann[2,*] H. H. Loosli,[2] I. L. Kamensky,[1] V. A. Nivin,[1] S. P. Orlov,[3] L. M. Ploschansky,[3] I. V. Tokarev,[4] and M. A. Gannibal[1]

[1]Geological Institute, Kola Scientific Centre of Russian Academy of Sciences, Apatity 184200, Russia
[2]Physics Institute, University of Bern, Bern 3012 Switzerland
[3]St. Petersburg Nuclear Physics Institute, Gatchina 188350, Russia
[4]Institute of Precambrian Geology and Geochronology, St. Petersburg 199164, Russia

(*Received July* 28, 1998; *accepted in revised form February* 26, 1999)

Abstract—Reduced ^{4}He/^{3}He ratios, e.g., down to ≈1/100 times those expected from radiogenic production, were observed in sedimentary rocks. Formation and history of these rocks eliminate a contribution of mantle ^{3}He-bearing fluid. To explain the difference between the observed and the calculated production ^{4}He/^{3}He ratios Loosli et al. (1995) and Tolstikhin et al. (1996) suggested a different behaviour of helium and tritium in damage tracks produced by emission of these nuclides. Generally, the tracks cross grain boundaries or some imperfections within a rock or mineral allowing a fast loss of noble ^{4}He and ^{3}He atoms. However, radiogenic ^{3}He has the precursor ^{3}H, generated in the exothermic ^{6}Li(n_t, α)^{3}H + 4.5 MeV reaction. The energetic tritons produce damage tracks comparable with those from α-decay of U and Th series. If ^{3}H is chemically bound within a track, and the track is able to recover via some diagenetic process before the ^{3}H decay, then ^{3}H and daughter ^{3}He atoms are trapped within the recovered track. This mechanism would explain the shorter residence time of ^{4}He in the rocks/minerals than of ^{3}He; therefore, ^{4}He/^{3}He ratios could decrease through time.

To check this mechanism ^{4}He, ^{3}H, and ^{3}He (from ^{3}H-decay) were produced by the above reaction in special targets, consisting of layered composites of thin sections of quartz, sample, Li-bearing cover, sample, and quartz. The samples were the same rocks in which reduced ^{4}He/^{3}He ratios have been previously observed. Each target was placed in a quartz ampoule, which was then pumped out, sealed off, and then exposed to the flux of thermal neutrons in a reactor. After irradiation and cooling down (total duration 145 days), the nuclides produced during (^{3}H, ^{3}He, ^{4}He) and after (^{3}He) irradiation were measured in the gas phase above the targets and compared with their total quantities expected from the Li abundance and the integrated neutron flux. The ratios obtained were ^{3}H(gas)/^{3}H(total) < 0.05 and ^{3}He(gas)/^{3}He(total) varying from 0.2 to 0.9. The average residence times τ of ^{3}H and ^{3}He, respectively, were estimated to be ≈16 and ≈0.25 yr for this first time interval, which included the irradiation of the targets.

After these first measurements, the targets were kept in a vacuum system under room temperature for 210 days and the amounts of ^{3}H and ^{3}He, which accumulated above the targets during this second time interval under fully controlled conditions, were also measured. Much slower rates of gas loss from the same targets with average residence times of $\tau(^3\text{H}) \approx 600$ yr and $\tau(\text{He}) \approx 1.6$ yr resulted for this second time interval. Probably these longer residence times are closer to those in the relevant natural environments, the ^{3}H residence time being much longer than the ^{3}H half-life.

In all cases the inequality $\tau(^3\text{He}) \ll \tau(^3\text{H})$ is valid. This confirms the proposed scenario envisaging longer retention of ^{3}H than He in damage tracks. Within the frame of this scenario the life-time of ^{3}H gives a time constraint on diagenetic processes; at least one to several newly formed atomic layers should appear during ~10 yr to recover the tracks. *Copyright © 1999 Elsevier Science Ltd*

1. INTRODUCTION

Noble gases are meaningful tracers of terrestrial fluids allowing investigation of the source of the fluids, the rate of their migration, and mixing and interactions with surrounding rocks. Among others helium appears to be of special importance (Mamyrin and Tolstikhin, 1984): (1) The dissipation of atmospheric He leads to extremely low abundance of He isotopes in air and related meteoric waters; therefore, rather small contributions of helium from host rocks or stagnant He-bearing fluids into young movable groundwaters can be detected (e.g., Kamensky et al., 1991). Helium is the most sensitive indicator of underground mixing processes. (2) The large difference between He isotope compositions in the mantle and crustal reservoirs allows a small contribution of mantle fluid to be recognised. (3) Production ^{4}He/^{3}He ratios depend on the major chemical composition, Li, and some trace element concentrations in host rocks; therefore, ^{4}He/^{3}He ratios in radiogenic helium are also used to identify sources of underground fluids.

Recently several researchers reported an intriguing controversy between ^{4}He/^{3}He ratios measured in some rocks and related underground fluids and those expected from radiogenic production. Hiyagon and Kennedy (1992) observed reduced ^{4}He/^{3}He ratios of $\sim (2 - 7) \times 10^6$ in methane-bearing gases from dolomite reservoirs capped by anhydrides in Alberta, Canada. Kennedy et al. (1992) also observed a reduced value of ^{4}He/^{3}He $= 1.7 \times 10^6$ unsupported by Li in anhydrite nodules from the Texas–Oklahoma Hugoton Gas Field.

*Author to whom correspondence should be addressed (lehmann@climate.unibe.ch).

Later on Loosli et al. (1995) and Tolstikhin et al. (1996) presented similar results for chemical sediments from sedimentary basins in Northern Switzerland; measured $^4He/^3He$ ratios down to 7×10^6 in dolomite and anhydrite from a borehole (Weiach) were by a factor of ~20 below the calculated values. These reduced ratios are noteworthy because release of He from such rocks/minerals can influence the ratio in groundwaters. Indeed, similar $^4He/^3He$ ratios were observed in Muschelkalk groundwaters.

Tolstikhin et al. (1996) discussed several mechanisms capable of reducing $^4He/^3He$ ratios in rocks and fluids and suggested a different retention of ^4He and ^3He as the most plausible effect. In fact, the parent isotope of ^3He is ^3H, which is produced in the exothermic $^6Li(n_t,\alpha)^3H$ reaction. Both ^4He (from U- and Th-α-decay) and ^3H are emitted with fairly large energies and produce damage tracks in the host mineral. ^4He is expected to escape easily along these tracks into crystal imperfections or grain boundaries (Gerling, 1957; Ashkinadze, 1980) where uranium and thorium usually reside (Komarov et al., 1982, 1985). ^3H might be chemically bound inside a track and therefore, much less mobile than an inert He atom. By the time ^3H decays to ^3He (tritium half-life is 12.26 a), the track could be recovered and ^3H becomes effectively trapped. The low energy available in the β-decay of ^3H might not be sufficient to liberate ^3He atoms from these recovered tracks. Such a mechanism requires the damage tracks to have a shorter life time in, for example, chemical marine sediments, than in some silicate minerals and oxides; annealing of tracks in carbonates and anhydrides at slightly elevated temperatures should proceed on a 10-yr time scale. This is in contrast to the 4.5-Ga long retention of ^{244}Pu fission tracks in various minerals separated from meteorites (Crozaz et al., 1989, and references therein).

Investigation of the mechanism of He isotope fractionation related to a specific behaviour of ^3H, the precursor of ^3He, is the major objective of this contribution. The species of interest, ^3H and ^4He, were produced by irradiation of Li-bearing targets with thermal neutrons; ^3He was then accumulating from ^3H decay. A comparison of the total amount of ^3H and $^{3,4}He$ produced by the irradiation with the fraction liberated from the target allows the residence times of these species to be obtained.

2. EXPERIMENTAL

2.1. The Targets

Targets prepared for the irradiation were "cakelike" layered composites of quartz glass/rock sample/Li-bearing layer/rock sample/quartz glass (Fig. 1). The quartz glass was used as a support plate for the rock samples. The quartz and rock sections were bound together by Canadian balsam or similar glue (Table 1). The rocks selected were the very same dolomite and anhydrites in which reduced $^4He/^3He$ ratios have previously been measured (Tolstikhin et al., 1996). Table 2 summarises some relevant data obtained for these rocks. Note that the average abundances of Li, ^4He, and ^3He in these samples are all much smaller than those in the targets after irradiation. In addition, a sample of man-made glassy quartz without rock slices was also used for comparison. The open surface of the rock section was covered by a Li-bearing layer either by sputtering of LiF in vacuum or by covering with thin layers of Li-bearing zinnwaldite from which rather thin slices were obtained by electric impulse desintegration (Semkin et al., 1995). The Li abundance in a target was determined either by interpolating Li concentrations obtained from adjacent quartz plates simultaneously covered by LiF during ion sputtering, or by measuring the Li concentration and the weight of mica used for a given target (Table 3). In both cases the concentrations of Li were determined by disintegration of the samples in acids, dissolution in distilled water, and spectrophotometric measurements. The repeated runs have shown a reproducibility of the analysis at $\pm 5\%$ (one σ is used hereafter).

All the slices were bound together by aluminum wire. Each target was placed in a quartz ampoule, which was subsequently evacuated and sealed.

2.2. Noble Gas Mass Spectrometry

The measurement of helium isotope abundances in rocks (minerals) was described in some detail by Kamensky et al. (1990, 1991) and Tolstikhin et al. (1996). From solid samples (Table 2) helium was extracted by stepwise heating or melting at 1600°C in a double-vacuum furnace. The glass ampoules (see Table 5 below) were opened in a specially designed ampoule-breaker. Ti-Zr getters were used to purify the noble gases; He (and Ne) was separated from Ar (and heavier gases) using charcoal traps, cooled by liquid nitrogen.

The isotopic composition and the concentration of helium were measured with a static mass spectrometer MI1201 22-78, which provided a complete separation of $^3He^+$ from the hydrogen doublet H_3^+ and HD^+. Standard gases were analysed before the measurements to calibrate the mass spectrometer; the only difference between standard and air gases was the abundance of helium. The ratio of He/Ne in the standard was 17.

Concentrations were measured by the peak height method with an accuracy of $\pm 7\%$. Uncertainties in $^4He/^3He$ ratios of $\sim 1 \times 10^6$ and 3×10^7 were about $\pm 2\%$ and $\pm 10\%$, respectively.

Blanks were measured after five runs. The total blank (the extraction system + the mass spectrometer chamber) was 1×10^{-9} cc STP for ^4He.

2.3. Irradiation and Gas Sampling

The quartz ampoules (all but one having targets inside) were irradiated in the nuclear reactor WWR-M of the St. Petersburg Nuclear Physics Institute. The mean flux of thermal neutrons and the release of energy were 2 to 6×10^{12} cm^{-2} s^{-1} and 0.04 to 0.1 W g^{-1}, respectively. Cooling water temperature was within 40 to 50°C. The integrated flux was measured using ^{60}Co monitors situated right nearby the targets. The flux accepted for each target was found by interpolation of the values obtained from the monitors. The accuracy of the flux measurements is ~10%.

After irradiation and cooling (termed hereafter as the first exposure interval whose duration was 145 days, see Fig. 2), the quartz ampoules were loaded into the stainless steel ampoule breakers. Attached to each ampoule breaker was a series of glass ampoules (≈0.2 L each) and small glass fingers filled with ≈0.1 g of activated charcoal. The entire apparatus was pumped out to a pressure of $<10^{-3}$ Torr. Once the vacuum was obtained the ampoule breaker and related ampoules were isolated from the vacuum pumping line, the ampoules were broken one by one, and the gas above each target was collected in the glass ampoules (Fig. 1), which were then sealed and used for analyses of tritium (Section 2.4) and helium (Section 2.2). The fraction of the total gas collected in each ampoule was determined from the volume ratio of V(ampoule)/V(total system), which was known to within ±10%.

All but one target were kept under vacuum (see Fig. 1) at room temperature for additional 210 days (termed as the second exposure interval) after which the sampling of gas above the targets and the measurements were repeated.

2.4. ^3H Measurements

The glass ampoule filled with the known portion of gas liberated from the target (Section 2.3) was loaded in an ampoule breaker connected to a SIK-32 ion chamber (7.2 L) and both were pumped out to a pressure of $\sim 10^{-1}$ Torr. The pumping line was then closed, the ampoule was broken, and air was admitted through the ampoule breaker carrying the sample gas from the broken ampoule into the chamber where the ^3H-induced ion current was measured with a voltmeter V7-45.

The background ion current of this device from cosmic rays and natural γ-radiation of construction materials was as low as $\sim 0.5 \times 10^{-14}$

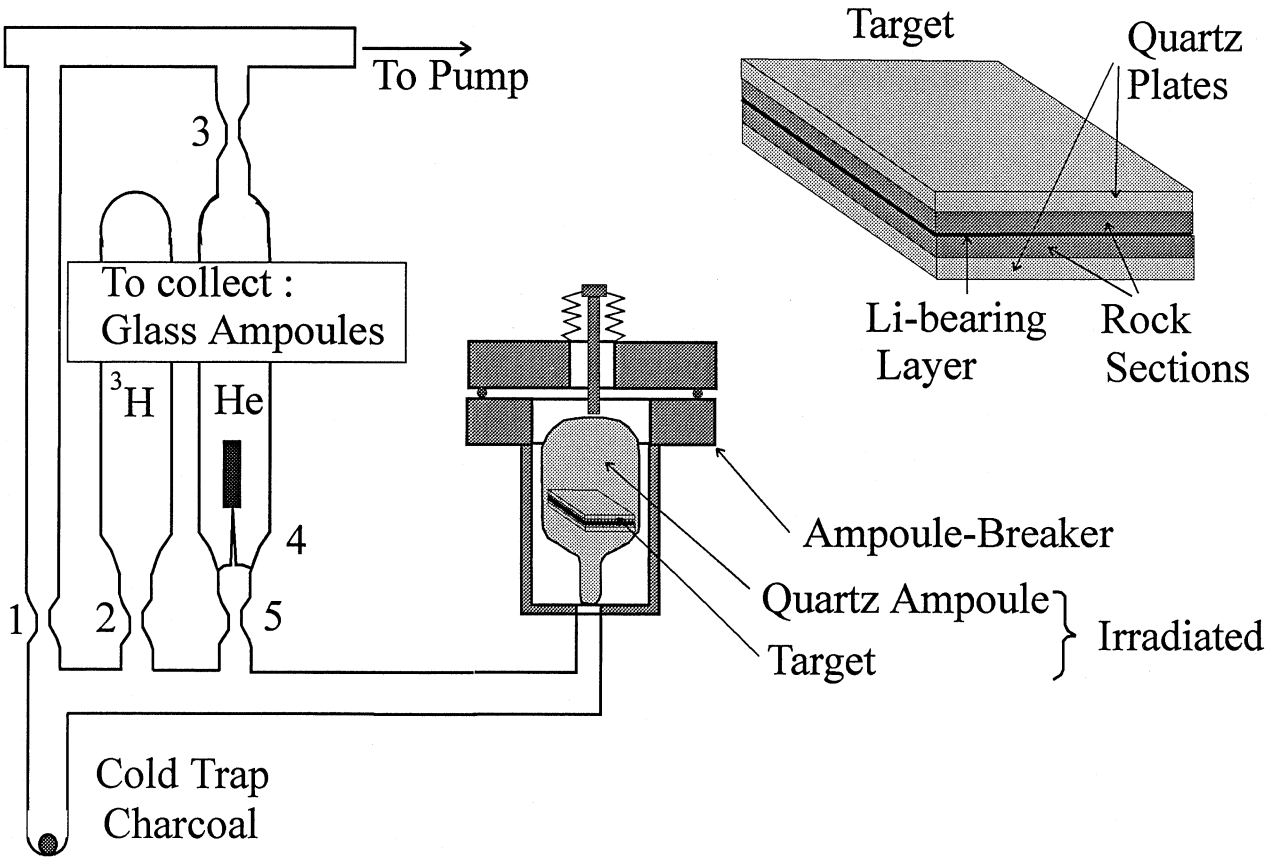

Fig. 1. Targets and vacuum system used to sample $^3H_{gas}$ and $^3He_{gas}$ from gas phase above the targets. A target (top right) is a composite of 10 × 10 mm slices; thickness, 0.2 mm for quartz plates, 0.05 mm for thin rock sections, or 0.1 mm for thick rock sections (Table 1) with Li-bearing layer between the rock sections. Each target was loaded in a quartz ampoule, pumped out and sealed off, then irradiated. Three months later each irradiated quartz ampoule was loaded in an ampoule-breaker (middle), the system was pumped out, capillary 1 was sealed, quartz ampoule broken, and gas was partitioned between the ampoule-breaker and ampoule "^{3}H" for 15 min. Then the "^{3}H" ampoule was sealed off (capillary 2) and used for ^{3}H measurement. Afterward capillary 3 was sealed, the cold trap was cooled down by liquid nitrogen, capillary 4 was broken, and He was admitted to the second ampoule "^{3}He" for 15 min, then the ampoule was sealed off (capillary 5) for He isotope analyses.

A, the sensitivity of ^{3}H measurements was 3.7×10^{16} Bq A^{-1}. The current of $\sim 0.5 \times 10^{-12}$ A, typical of our samples (see Table 4), was measured with an accuracy of ±6%.

3. RESULTS AND DISCUSSION

3.1. ^{3}H and ^{4}He Produced by Irradiation of ^{6}Li and ^{3}He From β-Decay of ^{3}H

The total ^{4}He* abundances [atoms] produced by irradiation were calculated from the Li amount [atoms] in an individual target (hereafter the superscript * indicates a calculated parameter) and the integrated flux of thermal neutrons Φ_t [cm^{-2}] by

$$^4He^*(t_{irr}) = Li\ \sigma_t\ \Phi_t \quad (1)$$

where σ_t is the cross section of the reaction 71×10^{-24} cm^2.

A similar equation, but taking into account the decay of ^{3}H during the irradiation time interval, t_{irr} = 0.15 yr (for all samples) gives

Table 1. The targets (see Fig. 1).

Index	Source of Li	Construction
A1	Zinnwaldite	Thin section of anhydrite is fixed on the quartz plate by Canadian balsam and starch is used to glue the mica on the surface of the anhydrite
A4	LiF vaporisation	Thin section of anhydrite is fixed on the quartz plate by Canadian balsam
A5	LiF vaporisation	Thick section of anhydrite is fixed on quartz plate by starch
A6	LiF vaporisation	Thin section of anhydrite is fixed on the quartz plate by Canadian balsam
D3	LiF vaporisation	Thin section of dolomite is fixed on quartz glass plate by starch
D5	LiF vaporisation	Thick section of dolomite is stuck on quartz glass by sugar syrup
Q1	LiF vaporisation	No glue used

Table 2. Abundances of Li, ^{3}He, and ^{4}He in anhydrides (AN) and dolomites (DM), the Weiach borehole, Molasse Basin, Northern Switzerland (from Tolstikhin et al., 1996, and unpublished data).

	Concentrations/Amounts		
Sample: Depth-Rock	Li (ppm)	^{4}He (cc STP/g $\times 10^{-6}$)	^{3}He (cc STP/g $\times 10^{-13}$)
942-AN	20	3.7	5.2
942-AN	20	4.0	4.4
941-AN	15	3.6	4.1
941-AN/DO	30	5.9	5.4
Average	21	4.3	4.9
Average (atoms/target)	5.5×10^{13}	3.5×10^{12}	3.9×10^{5}
819-DM	6.5	0.42	0.30
820-DM	6.0	0.47	0.65
824-DM	3.5	0.85	0.15
Average	5.3	0.58	0.83
Average (atoms/target)	1.4×10^{13}	4.7×10^{11}	6.7×10^{4}

$$^3H^*(t_{irr}) = (P/\lambda)\,[1 - \exp(-\lambda\, t_{irr})] \quad (2)$$

where $P = Li\ \sigma_t\ \Phi_t(t)$ is the production rate, λ is the decay constant of ^{3}H, $1.79 \times 10^{-9}\ s^{-1}$ (half-life $\tau = 12.26$ a $= \ln 2/\lambda$), and $\Phi_t(t)$ is the mean thermal neutron flux $\Phi_t(t) = \Phi_t/t_{irr}$.

Finally, ^{3}He produced by ^{3}H decay during the irradiation is determined by

$$^3He^*(t_{irr}) = Li\ \sigma_t\ \Phi_t(t)\,[t_{irr} - (1/\lambda)\{1 - \exp(-\lambda\, t_{irr})\}] \quad (3)$$

Table 3 summarises the calculated amounts of these nuclides at time t_{irr} when irradiation had been terminated. Because $^4He^*(t_{irr})$ is almost equal to $^3H^*(t_{irr})$, only the latter is shown.

3.2. Residence Time of ^{3}H in Target

After irradiation and cooling down ^{3}H was analysed in the gas phase above a target (Figs. 1 and 2, Table 4). Cooling of the glass finger (Section 2.3, Fig. 1) with liquid nitrogen resulted in a complete sorption of ^{3}H, therefore a sorbable compound appears to carry this nuclide.

Because of the high sorption capacity of the ^{3}H-bearing compound, control experiments were carried out to insure quantitative collection of ^{3}H in the glass ampoules. The ampoule breaker containing target A6 and the associated glass ampoule was pumped out and isolated from the pump, the quartz ampoule with the target inside was broken, and the gas was admitted to the glass ampoule for 15 min. The ampoule breaker, the connecting glass tubes, and the charcoal trap (see Fig. 1) were then heated (below 100°C) and the glass collection ampoule was simultaneously cooled with liquid nitrogen for another 15 min before it was sealed off. The amount of ^{3}H collected in this ampoule was only slightly elevated relative to the expected total production $^3H^*$ (see target A6 in Table 4) and the residence time of ^{3}H was found to be the same within the experimental errors (last two columns in Table 4). Also, after ^{3}H had been measured, the chamber was pumped out and ^{3}H still retained in the attached ampoule breaker was transferred by air to the chamber and measured. Again, only a negligible amount of ^{3}H was found in this repeated run (<0.03 of what was initially observed).

As an additional test, one of the irradiated targets (A1) was completely dissolved in HNO_3 after ^{3}H and ^{3}He in the gas phase had been analysed. Then, ^{3}H was measured in the solution by liquid scintillation counting. The resulting activity, 720 kBq, corresponds to 4×10^{14} ^{3}H atoms, in good agreement with the value calculated from the Li abundance and the neutron flux as presented in Table 3. All these control experiments confirm the ^{3}H data presented in Tables 3 and 4.

Table 4 and Figure 2 demonstrate definitely that the loss of ^{3}H from the targets to the gas phase is small ($\leq 5\%$) in all cases. It is not clear when and how ^{3}H was liberated. Some ^{3}H nuclides must escape the target during the irradiation (e.g., those produced from Li situated nearby the edge of the target). Also an enhanced loss of ^{3}H and ^{3}He during the irradiation could result from an elevated temperature (Section 2.4). Because this enhanced loss cannot be quantified, a constant loss rate is assumed hereafter for the first exposure interval.

The ^{3}H abundance in a target is determined by

$$d^3H/dt = P - \lambda\ ^3H - \alpha\ ^3H \quad (4)$$

where P is the production rate from Eqn. (2), λ is the ^{3}H decay constant, and α is the transport coefficient controlling the rate of ^{3}H loss from a target. The residence time of ^{3}H in a target is defined as $\tau(^3H) = \ln 2/\alpha$. The difference between the solid curve in Fig. 2 (calculated with $\alpha = 0$) and the dashed curve (calculated with $\alpha > 0$) represents the ^{3}H abundance in the gas phase. By varying α this difference was adjusted to the value measured at the end of the first exposure interval (Fig. 2). The ^{3}H residence times for several targets calculated from the respective α are listed in Table 4. Fig. 3 comprises all available

Table 3. Calculated quantities of $^3H^*(t_{irr})$ and $^3He^*(t_{irr})$ produced during irradiation.

Target	Li 10^{18} at	Error	Φ_t 10^{18} cm^{-2}	Error	$^3H^*(t_{irr})$ 10^{14} at	Error	$^3He^*(t_{irr})$ 10^{12} at	Error
A1	0.51	0.025	11	1	4.0	0.60	1.7	0.34
A4	1.8	0.09	6	0.6	7.7	1.10	3.3	0.49
A5	1.8	0.09	4.9	0.5	6.3	0.90	2.7	0.40
A6	3.6	0.18	0.36	0.04	0.94	0.14	0.40	0.06
D3	1.8	0.09	6	0.6	7.7	1.10	3.3	0.49
D5	1.l	0.06	4.9	0.5	3.9	0.60	1.7	0.25
Q1	1.8	0.09	6	0.6	7.7	1.10	3.3	0.49

The calculated values correspond to the time when irradiation was terminated.

Amounts of Li in Li-bearing layers, ^{3}H (and ^{4}He) expected from irradiation and ^{3}He from the decay of ^{3}H are always much greater than those in the thin sections of the rock samples themselves (Table 2). Therefore no correction was made for a contribution of these species from the samples.

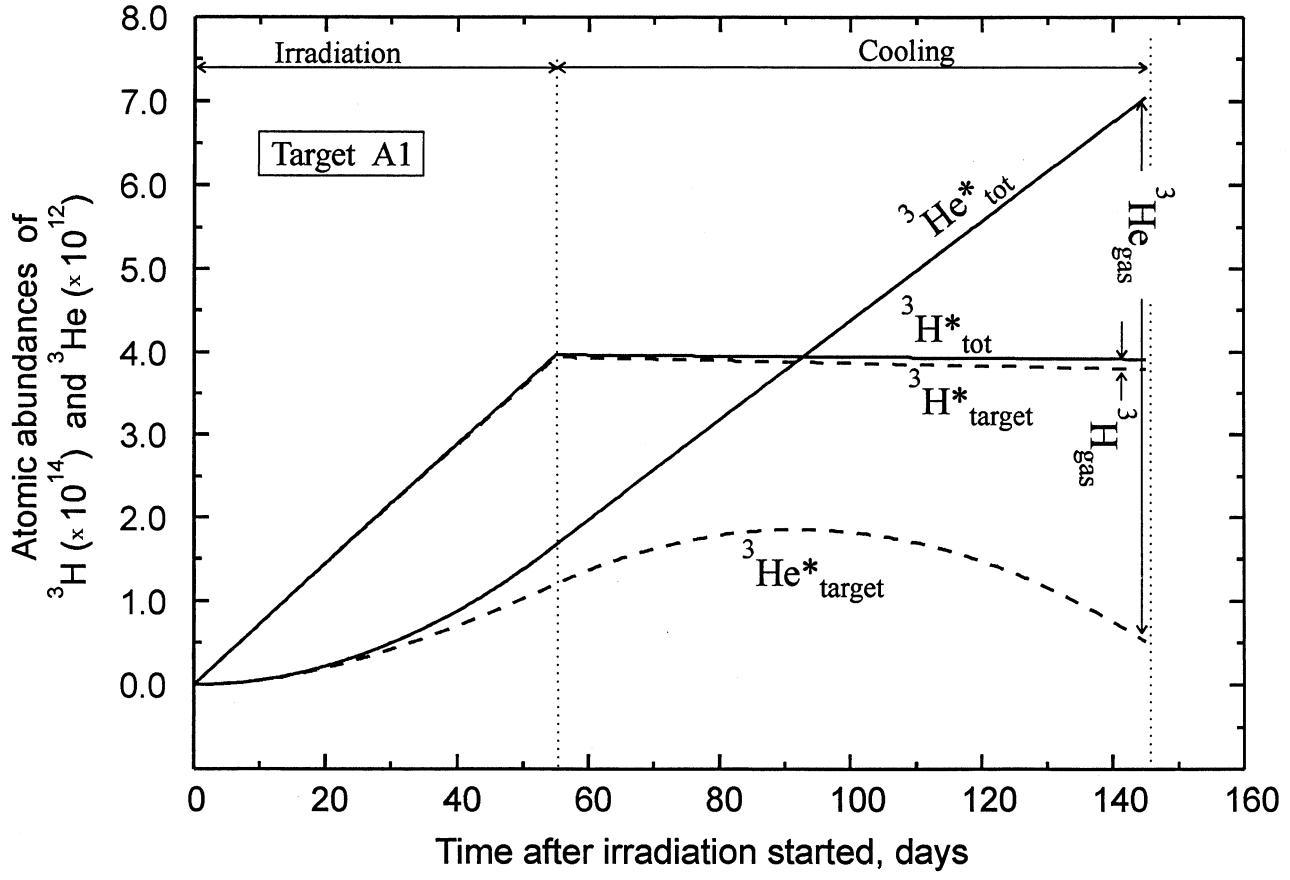

Fig. 2. Evolution of ^3H and ^3He in the irradiated samples. Solid lines represent the calculated total quantities in the system as a function of time; dashed lines show the amounts remaining in the targets taking into account losses to the gas phase. The difference between the two curves corresponds to the amount of the species in the gas phase, which was measured at the end of the first exposure 145-day long interval. For target A1 (selected for this Figure), ^3H and ^3He losses of 3.1% (Table 4) and 93% (Table 5) correspond to respective residence times of 0.12 yr and 7.2 yr.

$\tau(^3H)$ varying within a great range from 7 to 1400 yr (see discussion in Section 3.3).

3.3. Residence Time of He in Target: Comparison With ^3H Results

According to the principal reaction $^6Li(n_t,\alpha)^3H$, both ^4He and ^3H must be produced at the same rate. However, a comparison of Tables 3 and 5 shows that the measured quantities of ^4He in the gas phase always exceed the total amount of ^3H produced from the above reaction. Because the targets were enriched in Li and the cross section of the reaction is rather high, an additional considerable yield of ^4He from other nuclear reactions appears unlikely. Both quartz and Mo glass ampoules (Fig. 1) are highly penetrable for helium; therefore, the ^4He

Table 4. ^3H measured in the gas phase above the targets, comparisons with the amounts expected from irradiation, and the ^3H residence time $\tau(^3H)$.

Target	I_{meas} 10^{-13} A	Error	K_{vol} Ratio	Error	$^3H_{gas}$ 10^{13} at	Error	$^3H_{gas}/^3H^*_{tot}$	Error	$\tau(^3H)$ year	Error
A1	4.3	0.43	0.74	0.074	1.21	0.24	0.031	0.012	7.2	3.5
A4	5.4	0.54	0.74	0.074	1.51	0.30	0.020	0.007	11	4.5
A5	1.5	0.15	0.74	0.074	0.42	0.083	0.007	0.002	33	15
A6	1	0.1	0.45	0.045	0.46	0.092	0.050	0.018	6.4	2.7
D3	2.9	0.29	0.74	0.074	0.81	0.16	0.011	0.004	21	8.6
D5	2.9	0.29	0.74	0.074	0.81	0.16	0.021	0.007	10	4.1
Q1	2.6	0.26	0.74	0.074	0.73	0.14	0.010	0.003	23	9.5

^3H amount in the gas above the target was calculated by $^3H = (I_{meas}/K_{vol}) \times (S/\lambda)$, where I_{meas} is the measured ion current [A], S is the sensitivity of the ionisation chamber, $S = 3.7 \times 10^{16}$ [Bq A^{-1}], λ is the decay constant of ^3H [s^{-1}], and K_{vol} is the gas portion collected in a glass ampoule (Fig. 1) and used for the measurements.

^3H above all but one (A6) targets was analysed 90 days after the irradiation had been terminated, and ^3H above A6 was measured 150 day after irradiation. Results obtained after the second exposure interval are not included in the Table (see Fig. 3).

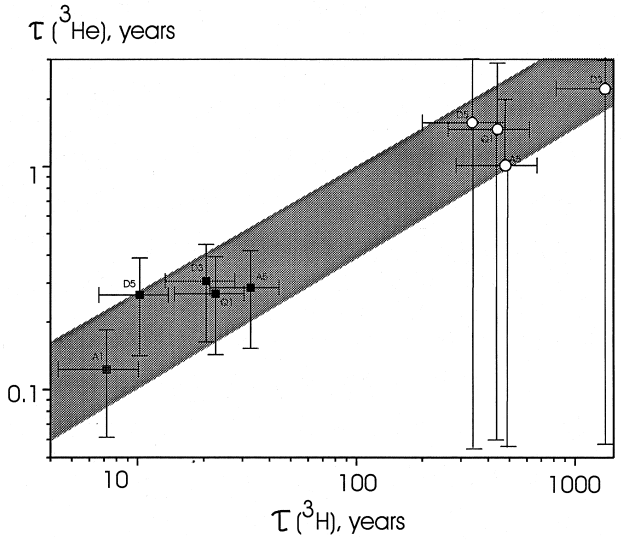

Fig. 3. Comparison of ^{3}H and ^{3}He residence times in targets. Squares and circles correspond to the residence times obtained for the first exposure time interval (145 days, including the irradiation) and for the subsequent second interval (210 days under fully controlled conditions), respectively. Notice that the inequality $\tau(^3\text{He}) \ll \tau(^3\text{H})$ is valid for each data point. The ^{3}H residence times for the second exposure interval are much longer than ^{3}H half-life. In the relevant natural environments even longer residence times are expected. Therefore, ^{3}H half-life constraints the damage track recovery on a time scale of ~10 yr.

excess arises most probably from air contamination. Because of a high amount of ^{4}He in the background experiment, this nuclide is used hereafter only as a measure of air contamination (target B1 in Table 5). Therefore, the residence time of He in a target was extracted from ^{3}He abundances.

Assuming the high ^{4}He in the background experiment represents air contamination, then the high ^{3}He/^{4}He ratio in the background experiment (see B1 in Table 5) implies a contribution of ^{3}He from Li impurities in quartz. Fortunately, the ^{3}He measured above a target exceeds the background quantity by a factor from 6 to 100,000 allowing reliable estimates of He residence time in the irradiated targets.

In contrast to ^{3}H, a substantial portion of ^{3}He had been lost from the targets into the gas phase before sampling and measurements (Fig. 3).

The ^{3}He abundance in a target is determined by

$$d^3\text{He}/dt = \lambda\, ^3\text{H} - \beta\, ^3\text{He} \qquad (8)$$

where β is the transport coefficient controlling the rate of ^{3}He loss from a target and the residence time of ^{3}He in a target is defined as $\tau(^3\text{He}) = \ln 2/\beta$.

As in the case with ^{3}H, the transport coefficient β was determined by adjusting the calculated difference between the ^{3}He accumulation with and without loss (Fig. 2) to the measured ^{3}He quantity in the gas phase and ^{3}He residence times were calculated from the respective β. Results obtained for the first exposure interval are listed in Table 5.

The residence times for ^{3}H and ^{3}He vary within a great range depending on the conditions of the experiments. ^{3}H and ^{3}He abundances in the gas phase after the first exposure interval (145 days) give low residence times as indicated by the left bottom group in Fig. 3, with the average values for this group at $\tau(^3\text{H})_1 = 16$ yr and $\tau(^3\text{He})_1 = 0.25$ yr.

The longer residence times are inferred for the subsequent second exposure interval (having a duration of 210 days), as presented by the right-top group of data points (Fig. 3). The average residence times for this group are $\tau(^3\text{H})_2 = 660$ yr and $\tau(^3\text{He})_2 = 1.6$ yr.

Obviously the difference between the two groups is related to some additional loss of ^{3}H and, to a lesser extent, ^{3}He during the irradiation time interval. The higher increase of the tritium residence time, $\tau(^3\text{H})_2/\tau(^3\text{H})_1 \approx 40$, as compared with helium, $\tau(^3\text{H})_2/\tau(^3\text{H})_1 \approx 6$, can be qualitatively explained by the different production times. ^{3}H was totally produced during the irradiation and its loss could be stimulated, for example, by heating of the Li-bearing layer, whereas ^{3}He was mainly yielded by ^{3}H decay afterward.

According to Fig. 3, the inequality $\tau(^3\text{He}) \ll \tau(^3\text{H})$ is valid for each data point, thus supporting the idea of ^{3}H/He(U,Th) fractionation as a result of much longer ^{3}H residence time in radiation tracks than that for radiogenic He.

Relationships between the residence times obtained in this study and those in the natural environments cannot be quanti-

Table 5. He isotope abundances in the gas above the targets, comparison with amounts expected from irradiation, and the He residence time τ.

Target	$^4\text{He}_{gas}$ 10^{14} atoms	Error	^{4}He/^{3}He	Error	$^3\text{He}_{gas}$ 10^{12} atoms	Error	$^3\text{He*}_{tot}$ 10^{12} atoms	Error	$^3\text{He}_{gas}/^3\text{He*}_{tot}$	Error	$\tau(^3\text{He})$ year	Error
(1)	(2)	(3)	(4)	(5)	(6)	(7)	(8)	(9)	(10)	(11)	(12)	(13)
A1	52	13	790	40	6.5	2.0	7	1.4	0.93	0.46	0.12	0.061
A4	44	17	270	13	16	7.2	14	2.1	1.14	0.68		
A5	34	9	760	38	4.5	1.4	11	1.7	0.41	0.19	0.29	0.13
D3	12	3	230	11	5.0	1.6	14	2.1	0.36	0.17	0.31	0.14
D5	25	7	860	43	2.9	0.92	6.8	1.0	0.43	0.20	0.27	0.12
Q1	27	7	460	23	5.8	1.8	14	2.1	0.41	0.19	0.27	0.13
B1	7	1	1600	78	0.43	0.10	—		—		—	

(2) Amount of ^{4}He above a target, $^4\text{He}_{gas} = {}^4\text{He}_{measured}/K_{vol}$, where $^4\text{He}_{measured}$ is the measured amount of ^{4}He in the glass ampoule and K_{vol} is the ratio between the volume of the glass ampoule and the total volume of the system as shown in Fig. 1. Errors shown includes both errors for $^4\text{He}_{measured}$ and K_{vol}.

(6) The ^{3}He background is much lower than the amounts of this nuclude above the targets, therefore no correction was made for the background.

(12) The residence time for sample A4 cannot be calculated because within the error bars all ^{3}He has been lost from the target.

Results obtained after the second exposure interval are not included in the Table (see Fig. 3).

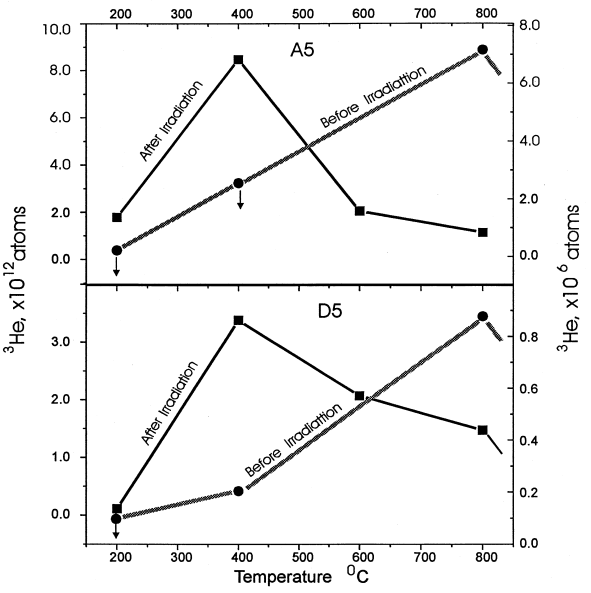

Fig. 4. Results of step-wise heating experiments for dolomite (D5) and anhydrite (A5) before and after irradiation. Right and left axes define ^{3}He amount in the temperature fractions before (circles) and after (squares) irradiation, respectively. Notice 10^6 times difference between the axes. Major ^{3}He loss from open radiation tracks occurs under ≈400°C. Integrated ^{3}He loss from both irradiated targets A5 and D5 agrees (within 2σ) with its amount expected from ^{3}H decay.

fied using available data. The longer τ appears to be a better choice because at least the two affecting factors accompanying the irradiation, heating of Li-bearing layer and spread out of the nuclides from edges of the targets, are eliminated. At first glance the results of the stepwise heating experiments imply a better preservation of ^{3}He in natural samples (i.e., before irradiation) (Fig. 4). However, the preirradiated samples do contain helium in recovered tracks or isolated vesicles only, whereas nucleogenic species in the targets occupy radiation tracks opened by (at least) one side to the Li-bearing layer. More work is needed to adapt the residence times obtained in Laboratory conditions to the natural environment. The promising results obtained in this study may stimulate this work.

4. SUMMARY

Our experiments demonstrate that the residence time of ^{3}H atoms generated by the ^{6}Li(n_t, α)^{3}H reaction inside an irradiated target is longer by a factor from 60 to 400 than that of ^{3}He atoms from the subsequent decay of ^{3}H. A considerable difference in ^{4}He and ^{3}He migration parameters is not expected and therefore, the residence time obtained for ^{3}He is most likely also valid for ^{4}He.

This preferential retention of tritium relative to helium is a first necessary process to support the explanation for the ^{3}He excess in certain rocks and minerals proposed by Loosli et al. (1995) and Tolstikhin et al. (1996). The average residence times of ^{3}H inside the targets obtained in this study exceed the ^{3}H half-life. The difference between the average $\tau(^3\text{H}) = 660$ yr obtained for the second exposure interval (which excluded the irradiation and the related specific ^{3}H loss) and the half-life of ^{3}H (12.3 yr), appears to be especially large. Moreover, even longer $\tau(^3\text{He})$ is expected in the natural environments because in our experiments the targets were in fact the natural samples but partially crushed by surface grinding and severe irradiation. If relatively long $\tau(^3\text{H})$ is the case, relationships between the laboratory-derived rates of ^{3}H migration and those under the natural conditions are not so important because the ^{3}H half-life constrains the radiation damage track recovery time scale; if the tracks in rocks/minerals are recovered on a time scale of ≈10 yr, ^{3}He atoms might not be able to migrate from their site of production. On the other hand, ^{4}He atoms produced by U and Th decay could escape on the time scale within 0.25 to 1.6 yr, causing a decrease of the ^{4}He/^{3}He ratio in the rock (mineral). After ^{3}He had been accumulating relative to ^{4}He, ^{3}He loss from recovered tracks through diagenetic or tectonic processes could temporally decrease ^{4}He/^{3}He ratios in related groundwaters.

Acknowledgments—The authors thanks Drs. V. Vetrin, S. Ikorsky, V. Skiba, Ya. Pakhomovsky, L. Gannibal, and A. Usov and technician N. Mashistova from the Geological Institute for their help in preparing the targets. Prof. K. Konoplev stimulated irradiation of the targets and investigation of radioactive samples in the St. Petersburg Nuclear Physics Institute; Dr. N. Khamov from this Institute also helped with these experiments. This study was supported by the Swiss National Science Foundation within the frame of the Swiss-Russian research collaboration project N-7SUPJ048649 "Helium and Argon Isotopes in Hydrology."

REFERENCES

Ashkinadze G. Sh. (1980) *Migration of Radiogenic Isotopes in Minerals* (in Russian). Nauka.

Crozaz G., Pellas P., Bourot-Denise M., de Chazal S. M., Fieni C., Lundberg L., and Zinner E. (1989) Plutonium, uranium and rare earths in the phosphates of ordinary chondrites—the quest for a chronometer. *Earth Planet. Sci. Lett.* **93,** 157–169.

Gerling E. K. (1957) Migration of helium from rocks and minerals (in Russian). *Trudy Radievigo Instituta, Acad. Nauk SSSR, Leningrad* **6,** 64–87.

Hiyagon H. and Kennedy B. M. (1992) Noble gases in CH_4 gas field, Alberta, Canada. *Geochim. Cosmochim. Acta* **56,** 1569–1589.

Kamensky I. L., Tolstikhin I. N., and Vetrin V. R. (1990) Juvenile helium in ancient rocks: I. ^{3}He excess in amphiboles from 2.8 Ga charnokite series—Crust–mantle fluid in intracrustal magmatic processes. *Geochim. Cosmochim. Acta* **54,** 3115–3122.

Kamensky I. L., Tokarev I. V., and Tolstikhin I. N. (1991) ^{3}H-^{3}He dating: A case for mixing of young and old groundwaters. *Geochim. Cosmochim. Acta* **55,** 2895–2899.

Kennedy B. M., Poths J., and Hiyagon H. (1992) Anomalous ^{3}He contents in CH_4-rich gases in sedimentary basins. In *Water–Rock Interaction* (ed. Kharaka and Maest), pp. 947–950. Balkema.

Komarov A. N., Sergeev S. A., Vardzelashvili N. S., and Pavshukov V. V. (1982) Quantitative radiographic analysis of uranium distribution in granites (in Russian). *Geokhimiya* **2,** 217–229.

Komarov A. N., Berman I. B., and Koltsova T. V. (1985) Radiographic study of distribution of uranium and thorium in some granulites (in Russian). *Geokhimiya* **7,** 979–987.

Loosli H. H., Lehmann B. E., Gautschi A., and Tolstikhin I. N. (1995) Helium isotopes in rocks, minerals and related groundwaters. In *Water–Rock Interaction* (ed. Y. K. Kharara and O. Chudaev), pp. 31–34. Proc. 8th International Symp. Water-Rock-Interaction, Vladivostok.

Mamyrin B. A. and Tolstikhin I. N. (1984) *Helium Isotopes in Nature.* Elsevier Sci.

Semkin B. V., Usov A. F., and Kurets V. I. (1995) *The Principles of Electric Impulse Destruction of Materials* (in Russian). Nauka, KSC RAS.

Tolstikhin I. N., Lehmann B. E., Loosli H. H., and Gautschi A. (1996) Helium and argon isotopes in rocks, minerals and related groundwaters: A case study in Northern Switzerland. *Geochim. Cosmochim. Acta* **60,** 1497–1514.